ELSEVIER

Biophysical Chemistry 129 (2007) 148–162

Biophysical Chemistry

http://www.elsevier.com/locate/biophyschem

Progress towards a DNA-based model system for the study of electron spin–spin interactions

Xi Jun Chen [a], Joseph Schramm [a], Christopher Tuohy [a], Heather Skiff [a], Kathleen Hummel [b], Anne R. Szklarski [a], Nicholas Vacirca [c], Bruce A. Wolf [d], Donald J. Hirsh [a,*]

[a] Department of Chemistry, The College of New Jersey, PO Box 7718, Ewing, NJ 08628, United States
[b] Department of Physics, The College of New Jersey, PO Box 7718, Ewing, NJ 08628, United States
[c] Department of Electrical Engineering, The College of New Jersey, PO Box 7718, Ewing, NJ 08628, United States
[d] Department of Mechanical Engineering, The College of New Jersey, PO Box 7718, Ewing, NJ 08628, United States

Received 26 March 2007; received in revised form 22 May 2007; accepted 23 May 2007
Available online 31 May 2007

Abstract

A DNA-based model system is described for studying electron spin–spin interactions between a paramagnetic metal ion and a nitroxide spin label. The modified base deoxythymidine-EDTA (dT-EDTA) chelates the divalent or trivalent metal ion and produces a new feature in the circular dichroism (CD) spectra that makes it possible to monitor local DNA melting. Based on the results of optical and electron paramagnetic resonance (EPR) experiments, we find that the terminus of the DNA duplex that incorporates dT-EDTA and the spin-label melts at a higher temperature than the rest of the DNA duplex. EPR microwave progressive power saturation experiments performed at 77 K are consistent with the specific binding of Dy(III) at the EDTA site and an intramolecular dipole–dipole interaction between the nitroxide spin-label and the chelated Dy(III). This model system should be suitable for studying the relaxation properties of metal ions by saturation-recovery EPR.
© 2007 Elsevier B.V. All rights reserved.

Keywords: DNA melting; dT-EDTA; Circular dichroism; Electron paramagnetic resonance; Dipole–dipole interaction; Correlation times

1. Introduction

Distances between paramagnetic metal ions and either endogenous or exogenous radical species can be determined by the method of saturation-recovery EPR and this method has been applied to a number of proteins and protein complexes [1,2]. To our knowledge this methodology has not been applied to the study of nucleic acid or protein/nucleic acid structure, even though the potential exists for the substitution of Mn(II) and other paramagnetic cations for the native diamagnetic cations normally associated with these structures [3]. Our ability to apply this methodology to both proteins and nucleic acids is limited by our current knowledge of the spin-lattice (T_1) and spin–spin (spin-dephasing) (T_2) relaxation behavior of the metal ions themselves, particularly those with spin greater than one-half [4,5].

The paramagnetic properties of a metal ion or complex can be probed indirectly by observing its effect on the relaxation behavior of a radical a fixed distance away [6–9]. While protein-based and purely synthetic model structures have been used successfully to explore metal-ion–radical interactions [4,10–14], they are time-intensive to produce and purify. A general-purpose scaffold that could hold a radical and a variety of metal ions or metal complexes a fixed distance apart would offer a rich source of information on the relaxation properties of metal ions.

Duplex DNA has many properties that make it an attractive scaffold for a model system. First, the structure of duplex DNA is well characterized and identifiable by circular dichroism [15]. Second, the distance between a paramagnetic metal ion(s) and a radical can be varied by a number of strategies. If a ligand for the paramagnetic metal ion is attached to one strand and the

* Corresponding author. Tel.: +1 609 771 2463; fax: +1 609 637 5157.
E-mail address: hirsh@tcnj.edu (D.J. Hirsh).

0301-4622/$ - see front matter © 2007 Elsevier B.V. All rights reserved.
doi:10.1016/j.bpc.2007.05.014

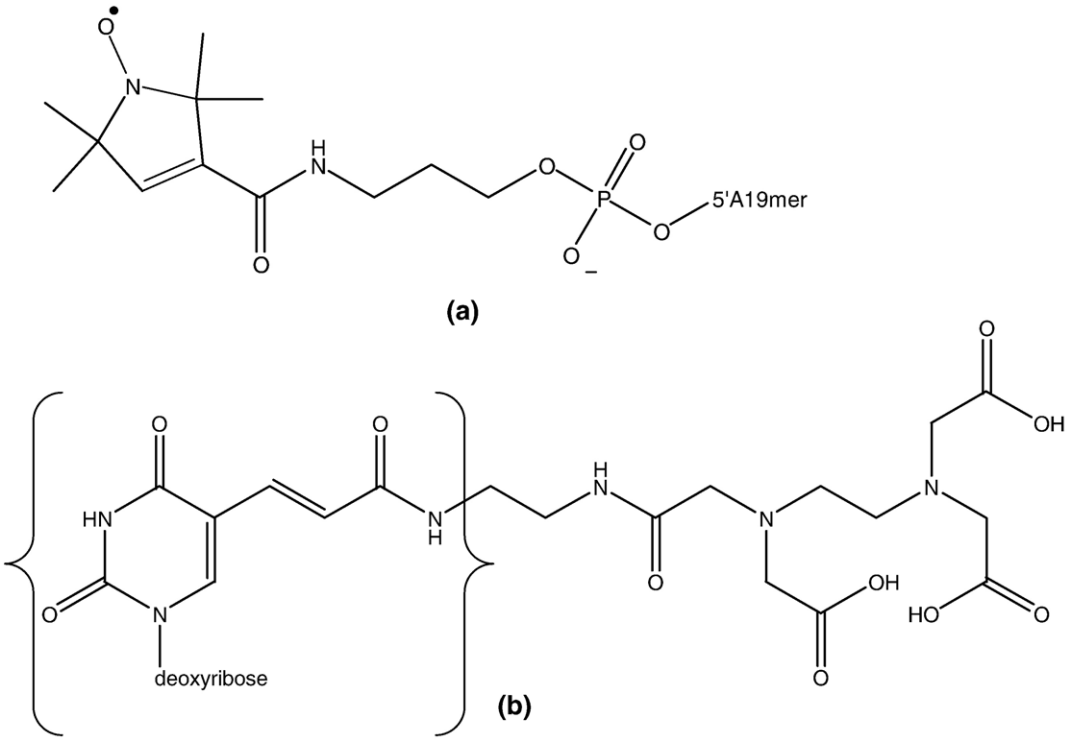

Fig. 1. (a) Attachment of the nitroxide spin-label, 1-Oxyl-2,2,5,5-tetramethylpyrroline-3-carboxylate, to the A19mer oligonucleotide. An aminoC3 "linker" ($H_2NCH_2CH_2CH_2OPO_3$) is attached to the 5′ end of the A19mer oligonucleotide by solid-phase phosphoramidite chemistry. An amide bond is then formed between the linker and the spin-label. (b) Structure of dT-EDTA. The structure within brackets is predicted to be planar and, based on experimental data described in this work, the exocyclic π electrons in this portion of the dT-EDTA linkage are coupled to those in the pyrimidine ring.

radical is attached to the complementary strand, the distance between a bound paramagnetic metal ion and the radical can be varied by mixing complementary strands that differ in the point(s) of attachment, by changing the sequence of bases in the two strands, and/or changing the length of the DNA duplex. Third, a chelator such as EDTA allows for a wide variety of paramagnetic metal ions to be incorporated into the model system and an EDTA derivative of deoxythymidine (dT-EDTA) is commercially available [16]. Fourth, since DNA is a polyanion, it should remain dispersed in solution, ensuring that only pair-wise interactions are observed. Finally, custom oligonucleotide synthesis is widely available.

We present here the physical characterization of a 19 base-pair DNA duplex containing dT-EDTA (E) and nitroxide spin-label (SL) on complementary strands (see below) and compare its spectroscopic and thermodynamic properties with those of the corresponding native and singly modified DNA duplexes. This doubly-labeled DNA duplex is identified as the SE-duplex. The labeled strands are identified as the SL-A19mer and the E-T19mer. In the SL-A19mer, the nitroxide spin-label,

5′ SL – GCATAGATACATAGATACG SL – A19mer

3′ CGTATCTATGTATCTATGC E – T19mer

1-Oxyl-2,2,5,5-tetramethylpyrroline-3-carboxylate, is connected to the A19mer via an amide linkage to a 3-carbon chain at its 5′ end, Fig. 1(a). In the E-T19mer, the chelator ethylenediaminetetraacetic acid (EDTA) is covalently attached to the C5 position of a deoxythymidine (dT) analog referred to here as dT-EDTA, Fig. 1(b). Its position at base 15 in the E-T19mer is marked by the symbol T (see sequence above). The binding of Dy(III) or Ca(II) ions at the EDTA moiety produces the SEDy- and SECa-duplexes, respectively. For future reference, these three DNA duplexes are shown schematically in Table 1. The asterisk (*) represents the spin-label and the box (□) represents the EDTA moiety.

In the *absence* of chemical modifications, we identify the DNA base sequence of the top strand as the A19mer and that of

Table 1
DNA duplexes

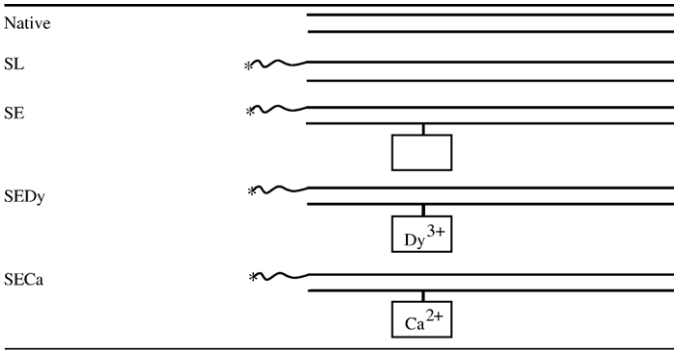

the bottom strand as the T19mer. Together, these two strands form the native duplex. Also examined in this work was the SL-duplex in which the SL-A19mer and the (unlabeled) T19mer were paired. This DNA duplex is identified as the SL-duplex. These two DNA duplexes are also shown schematically in Table 1. Note that the complementary strands in all 5 DNA duplexes shown in Table 1 have the base sequences shown above. What distinguishes the duplexes from each other are the presence or absence of covalently linked EDTA, covalently linked nitroxide spin-label, and/or bound metal ion.

We find that the conjugated linker region of dT-EDTA alters the absorption and CD properties of the thymidine chromophore such that it can serve as a local reporter of DNA structure and thermodynamics. Based on measures of both global and local DNA structure, the terminus of the DNA helix that includes dT-EDTA and the nitroxide spin-label has a higher melting temperature than the rest of the helix when either Ca(II) or Dy(III) are present. While the EDTA-moiety is attached to its DNA strand by a flexible tether in the SE-duplex, the experimental results indicate that it complexes with the DNA helix when either Ca(II) or Dy(III) is present. Finally, both the CD and EPR data are consistent with the Ca(II) and Dy(III) ions binding specifically to the EDTA moiety. These observations indicate that this DNA-based model system will be a suitable platform for studying electron spin–spin interactions between radicals and paramagnetic metal ions.

2. Experimental

Phosphate buffer reagents – potassium dihydrogen phosphate and potassium hydroxide, cryoprotectants – ethylene glycol (EG) and polyethylene glycol 6000 (PEG 6000), and the dipotassium salt of the chelator ethylenediaminetetraacetic acid were purchased from Acros Organics/Fisher Scientific International. The solvent N,*N*-dimethylformamide (DMF) was purchased from EMD, Darmstadt, Germany. The spin-labeling reagent, 1-Oxyl-2,2,5,5-tetramethylpyrroline-3-carboxylate, *N*-hydroxysuccinimide ester, was purchased from Toronto Research Chemicals, Inc., Ontario, Canada. The remaining reagents, dysprosium chloride, calcium chloride, PIPES free acid, *N*-(2-Hydroxyethyl)ethylenediamine-*N*,*N*′,*N*′-triacetic acid trisodium salt hydrate (HEDTA), dimethylsulfoxide (DMSO), triethylamine, and acetonitrile were purchased from Sigma-Aldrich, St. Louis, MO.

Unmodified DNA oligomers, dGCATAGATACATAGATACG (A19mer) and dCGTATCTATGTATCTATGC (T19mer) and the modified DNA oligomer ($H_2NCH_2CH_2CH_2PO_4$)-dGCATAGATACATAGATACG, (5′aminoC3-A19mer) were synthesized and HPLC purified by Operon Biotechnologies, Inc, Huntsville, AL. The modified DNA oligomer dCGTATCTATGTATCTATGC (EDTA-T19mer) where T = dT-EDTA was synthesized and purified using PAGE and reverse-phase HPLC by TriLink BioTechnologies, San Diego, CA. The E-T19mer was analyzed using a Dionex DNA PAC PA-100 4 × 250 mm anion exchange column at 60 °C and a linear gradient of 0–50% Buffer B over 20 min at a flow rate of 1 mL/min. Buffer A was 25 mM Tris, pH 9–10 and Buffer B was 25 mM Tris, pH 9–10, 2 M LiBr. In these analyses, the E-T19mer oligonucleotides represented between 95 and 98% of the total DNA present.

2.1. Determination of extinction coefficients of A19mer and T19mer

The molar absorptivities or extinction coefficients at 260 nm, ε_{260}, of these two oligonucleotides were determined by the method of Kallansrud and Ward [17], using snake venom phosphodiesterase. Extinction coefficients were determined on the basis of three trials on the native A19mer and T19mer and were found to be 173 ± 2 and 159 ± 2 $mM^{-1}\cdot cm^{-1}$, respectively. The extinction coefficients of SL-A19mer and EDTA-T19mer were assumed to be the same as those of the native oligomers.

2.2. Synthesis of spin-labeled A19mer (SL-A19mer)

A 1.0 mM solution of 5′AmC3-A19mer was made by the suspension of the DNA in 200 mM borate buffer, pH 9.0. An equal volume of the *N*-hydroxysuccinimide (NHS) ester of the nitroxide spin label was added at a concentration of 100 mM in

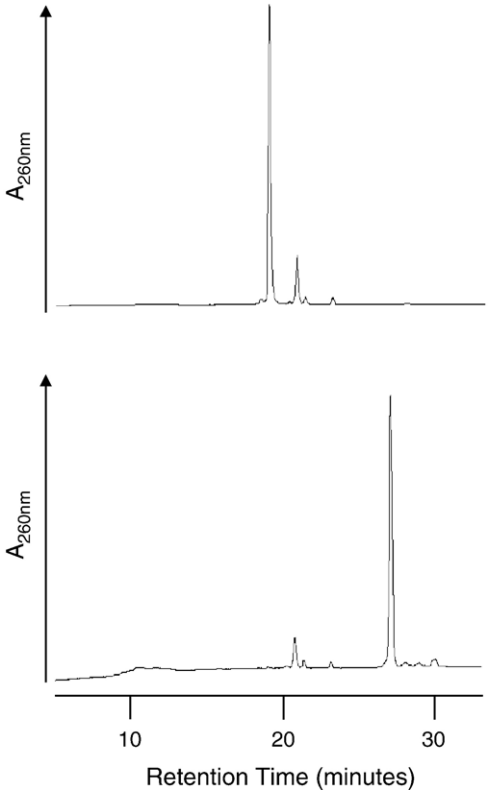

Fig. 2. Analysis of (a) 5′-aminoC3-A19mer (retention time = 19 min) and (b) SL-A19mer (retention time 27 min) was performed by reverse-phase HPLC. A peak with a retention time of 20.7 min appears in both chromatograms and probably represents full-length A19mer that was not conjugated by aminoC3, ($H_2NCH_2CH_2CH_2PO_4$), in the final step of solid-phase synthesis. Analysis was performed with a Varian ThermaSep, 100 Å, 5 micron, 4.6 × 250 mm reverse-phase HPLC column operating at 70 °C. Separation of the components was achieved with a flow rate of 1 mL/min and a linear gradient of 6–22% Buffer B over 24 min. Buffer A was 95:5, 100 mM triethylammonium acetate (TEAA) pH 7:acetonitrile and Buffer B was 50:50, 100 mM TEAA pH 7:acetonitrile.

Table 2
Hyperchromism and changes in circular dichroism in PIB-cryoprotectant

DNA duplex	% Hyperchromism		$\Delta[\theta_{248\ nm}]$/mdeg		$\Delta[\theta_{310\ nm}]$/mdeg	
	Total	Melt	Total	Melt	Total	Melt
Native	24.6±0.4	24.5±0.4	17.7±0.3	13.3±0.1	–	–
SL	24.2±0.8	23.3±0.7	17.0±0.3	13.5±0.4	–	–
SEDy	22.3±0.2	20.9±0.8	16.9±0.5	13.4±0.2	2.4±0.2	1.83±0.03
SECa	21.8±0.2	20.8±0.9	16.4±0.3	13.1±0.3	2.3±0.1	1.77±0.03

DMSO. Fresh DMF was added in equal volume to the buffer and DMSO to aid the dissolution of the NHS ester of the nitroxide spin-label. The resulting reaction mixture was vortex mixed and placed in a covered, temperature-regulated water bath at 37 °C overnight. The spin-labeled DNA was purified by gel-filtration chromatography using a PD-10 Desalting Column (GE Healthcare/Amersham Biosciences, Uppsala, Sweden) equilibrated with 0.1 M triethylammonium acetate (TEAA) buffer, pH 7. The eluant from this column was collected in 0.5 mL fractions that were analyzed by ultraviolet spectroscopy and HPLC. Fractions free of excess spin-label were pooled, split into multiple microcentrifuge tubes, and dried using a vacuum centrifuge. As determined by HPLC, the yield of SL-A19mer from 5′aminoC3-A19mer was typically ≥90% with SL-A19mer DNA representing ~86% of the total DNA in the purified product, Fig. 2.

2.3. Spin-label/A19mer ratio

Purified SL-A19mer was resuspended in phosphate buffer and the concentration of DNA was determined based on its absorbance at 260 nm and its experimentally determined extinction coefficient. TEMPOL, a stable, water soluble nitroxide radical with a known extinction coefficient was used to prepare standard solutions for EPR spectroscopy [18]. Glass micropipettes, 50 μL, were flame-sealed at one end and filled with 50 μL aliquots of the TEMPOL or SL-A19mer solutions. EPR spectra of these samples were collected and integrated twice to determine the area under the curve [19,20]. A calibration curve of area versus concentration was created using the TEMPOL solutions and used to determine the concentration of spin label (nitroxide radical) in the SL-A19mer solution.

CW EPR spectra were collected at Swarthmore College using a Bruker EMX ESR spectrometer (Bruker Biospin, Billerica, MA) operating at X-band. EPR spectra were collected with microwave power in the linear response region (signal doubling with every 4× increase in microwave power) but the field modulation was allowed to exceed the intrinsic linewidth of the nitroxide signals in order to improve the signal-to-noise ratio [21]. The field modulation frequency was 100 kHz.

2.4. Preparation of DNA duplexes

Single-stranded DNA was suspended directly in either buffer or buffer-cryoprotectant (55/30/15, buffer/PEG 6000/ethylene glycol, w/w/w) at a concentration of 113 μM. Appropriate volumes of two complementary strands were then combined to form a solution that was 1:1, mole/mole, of the two strands and 56.5 μM in duplex DNA. Some initial work was done with 100 mM potassium phosphate, pH 7.0 (POB) as the buffer component. However, unless otherwise noted, all measurements in this report were performed with 50 mM PIPES, 85 mM NaCl, pH 7.0 (PIB) as the buffer. Both buffers have an ionic strength of 200 mM. Prior to performing DNA melting experiments to determine T_m and $\Delta H°$, all DNA duplexes were melted and annealed in 1 mm path length quartz cuvettes (Starna Cells, Inc., Atascadero, CA) using a Varian Cary 100 UV-VIS spectrophotometer (Varian Instruments, Walnut Creek, CA), a temperature range of 20–85 °C, and a heating/cooling rate of 0.8 °C/min.

Calcium and dysprosium ions were incorporated into the SECa- and SEDy-duplexes prior to melting and annealing by placing 1.05 equivalents of aqueous $CaCl_2$ or $DyCl_3$ into a microcentrifuge tube, removing the water by vacuum centrifugation, and then adding the appropriate volume of 56.5 μM SE-duplex in PIB-cryoprotectant to the dry $CaCl_2$ or $DyCl_3$. The paramagnetic metal ion Dy(III) was chosen for these studies because it significantly enhances the relaxation of radicals at cryogenic temperatures and the mechanism of its relaxation enhancement is believed to be understood [22,23]. For the SE-duplex, 1 mM EDTA was present in the PIB-cryoprotectant buffer solution in order to complex any adventitious divalent or trivalent cations that might otherwise bind to dT-EDTA.

2.5. UV-monitored and CD-monitored melting experiments

Combined UV-monitored and CD-monitored melting experiments were performed using a JASCO J-810 spectropolarimeter (Jasco, Inc., Easton, MD). Circular dichroism and absorbance were recorded every 1 nm from 350 to 220 nm at a scan rate of 100 nm/min. Complete spectra were recorded every 1 °C over a temperature range of 10–70 °C. Baseline spectra of the corresponding buffer or buffer-cryoprotectant solutions collected at 20 °C were subtracted from the CD and UV spectra of the DNA duplexes. The heating rate between spectra was 0.8 °C/min. Including the time required to collect a spectrum, the net heating rate was 0.3 °C/min. A slower heating rate of 0.4 °C/min between spectra was tested and found to yield the same values for T_m and $\Delta H°$. The experimental results reported in Tables 2 and 3 reflect the average and standard deviation for three trials.

2.6. Spin-label dynamics

The free spin-label and the SL-, SE-, SEDy-, and SECa-duplexes were in PIB-cryoprotectant at a concentration of

Table 3
Thermodynamics of DNA Melting in PIB-cryoprotectant

DNA duplex	T_m/°C			$\Delta H°$/kJ mol^{-1}		
	$A_{260\ nm}$	$[\theta_{248\ nm}]$	$[\theta_{310\ nm}]$	$A_{260\ nm}$	$[\theta_{248\ nm}]$	$[\theta_{310\ nm}]$
Native	53.0±0.3	52.6±0.3	–	389±4	404±5	–
SL	50.7±0.3	50.7±0.2	–	391±18	393±21	–
SEDy	51.3±0.4	51.1±0.2	52.6±1.1	341±13	329±12	438±31
SECa	50.8±0.5	51.1±0.4	52.3±0.5	325±4	341±3	458±24

56.5 μM. In the case of the DNA duplexes, the samples had been subjected to at least three cycles of melting and annealing. A 30 μL aliquot of each solution was loaded by syringe into a 50 μL glass micropipette flame-sealed at one end. The glass capillaries were placed inside an EPR tube and the EPR tube was capped with an air-tight seal prior to experimental measurements. Temperature control was achieved using a gas flow system. Liquid nitrogen boil-off provided dry nitrogen to an FTS Systems, Inc., XR401 Air Jet Sample Cooler. The temperature-regulated nitrogen gas was delivered to the EPR sample through a quartz Dewar insert purchased from Wilmad Glass Co. The temperature was monitored by a thermocouple mounted just below the EPR cavity. Calibrations performed with a thermocouple at the sample position indicated that temperatures recorded by the mounted thermocouple were within 0.2 °C of the actual sample temperature.

CW EPR spectra were collected at The College of New Jersey using a Bruker/IBM ER200D ESR spectrometer with a TM4103 cavity. On this instrument, spectra were collected using a home-built computer interface based on a National Instrument/LabView platform. EPR field modulation was 0.4 G and 100 kHz. EPR power was 816 μW, within the regime where the EPR signal doubles for each 4-fold increase in power.

2.7. Microwave progressive power saturation EPR experiments

Prior to loading into EPR tubes, all DNA duplexes had been subjected to at least three cycles of melting and annealing. Samples were prepared by loading 100 μL aliquots of 56.5 μM DNA duplex in PIB-cryoprotectant into quartz EPR tubes and rapidly cooling the DNA solution in liquid nitrogen. This process yielded a transparent glass. During data collection, the sample temperature was kept at 77 K using a quartz finger Dewar (Wilmad Glass Co.) filled with liquid nitrogen. Spectra were collected on the IBM ER200D ESR spectrometer with field modulation of 3.2 G amplitude and 100 kHz frequency.

3. Results

Our goal is to have a platform that can be used to study the spin–spin interactions of the nitroxide radical with a variety of metal ions, therefore we used Ca(II) and Dy(III) to test the sensitivity of the model system's structure to changes in metal ion size and valence. Since the saturation-recovery EPR experiments will be conducted at cryogenic temperatures, we chose to study the model system's structure and thermodynamics in the same buffer-cryoprotectant solution that will be used for future saturation-recovery EPR experiments. Finally, we wanted to determine if divalent and trivalent metal-ion binding occurred specifically at the dT-EDTA moiety.

3.1. Buffer-cryoprotectant glass

Various combinations of phosphate buffer (POB), PEG 6000, and ethylene glycol (EG) were tested to determine if they would form a transparent glass when rapidly cooled in liquid nitrogen. A transparent glass is presumably homogeneous and free of ice crystals, which could denature the DNA [24]. All solutions were at least 50% buffer by weight. Two distinct formulations met this requirement: 50:50, w/w, POB/PEG 6000 and 55:30:15, w/w/w, POB/PEG 6000/EG. The native duplex was suspended in both of these solutions and UV-monitored melting experiments were performed. Compared to phosphate buffer alone, T_m of the native duplex was 19 °C lower in the two-component solution containing PEG 6000 as the only cryoprotectant and 9 °C lower in the three-component solution containing both PEG 6000 and EG. Another disadvantage of the two-component POB/PEG 6000 buffer-cryoprotectant solution was its high viscosity. All subsequent buffer-cryoprotectant solutions were made with a three-component, 55:30:15, w/w/w, buffer/PEG 6000/EG composition.

3.2. Synthesis and purification of SL-A19mer

For synthetic simplicity and to avoid any perturbation to the helical structure of the DNA duplex, the nitroxide spin-label was conjugated to the 5′ end of the A19mer. A short linker available from Operon Biotechnologies, aminoC3, was used (see Fig. 1). Reaction of the NHS ester of the nitroxide spin-label, 1-Oxyl-2,2,5,5-tetramethylpyrroline-3-carboxylate, with the 5′-aminoC3-A19mer yielded the SL-A19mer. As shown in Fig. 2, spin-labeling of 5′-aminoC3-A19mer is essentially quantitative with the SL-A19mer representing >90% of the full length DNA and 86% of the total DNA present. The amide linkage of the spin-label to the DNA was quite robust. A three month old sample of SL-duplex that had been subjected to three UV-monitored melting experiments, and three cycles of freezing and thawing showed the same HPLC elution profile as that of a freshly made sample.

Because of the large excess of spin-label used in the synthesis of the SL-A19mer, we were careful to check for excess spin-label after gel-filtration of the reaction mixture. The diode-array detector used to monitor the elution of the SL-A19mer from the HPLC column at 258 nm was also used to monitor absorbance at 244 nm and 280 nm, the absorbance maxima of the hydrolyzed nitroxide spin-label and *N*-hydroxysuccinimide, respectively. However, we did not detect absorbance peaks from either of these reaction side products. In addition, we determined the spin-label/A19mer ratio as described in the Experimental section. Based on the EPR measurements and UV absorbance, the ratio of spin-label to A19mer was 0.85± 0.05:1, consistent with the HPLC results and with a one-to-one labeling of the 5′aminoC3-A19mer.

3.3. Selection of buffer

Inorganic phosphate forms insoluble complexes with a number of the metal ions we were interested in studying. Therefore we looked for an alternative buffer to use in these experiments. One of the properties of phosphate buffer that makes it so useful in determining the thermodynamic parameters associated with DNA duplex melting is the modest temperature dependence, $\Delta pK_a/\Delta T = -0.0028/°C$ [25], of its second pK_a (7.20). Typically, if metal complexation is a problem, cacodylic acid is used in place

of phosphate (phosphoric acid) because its pK_a is also weakly dependent on temperature. However, it is also toxic and we were reluctant to employ it in these studies.

We turned instead to one of the "Good" buffers [26], piperazine-*N*,*N*-bis(2-ethane-sulfonic acid), or PIPES. PIPES buffer has a pK_a of 6.8 at 25 °C and no reported metal binding capabilities. The temperature coefficient of its pK_a is greater than that of phosphate but still relatively small at $\Delta pK_a/\Delta T = -0.0085$/°C [27]. There were two concerns about using PIPES. First, the reported temperature coefficient appears to be based on its change in pK_a over a narrow temperature range, possibly 25–37 °C [27], and it was unclear if this temperature dependence remained constant above 37 °C. Second, it was uncertain that when mixed with cryoprotectants and subjected to repeated heating and cooling, the PIPES buffer would maintain its transparency in the UV region and its buffering capacity. To address the first concern, PIB, a PIPES/NaCl buffer solution was titrated to pH 7.0 at room temperature and then its pH was measured every 10 °C as it was heated to 80 °C. As expected, the pH dropped by ~0.085 pH units with each 10 °C increase in temperature. At 80 °C, the pH measured 6.46, precisely the value predicted based on the starting pH and the literature temperature coefficient of the pK_a. To address the second concern, PIB-cryoprotectant was subjected to four cycles of heating and cooling at a rate of 0.8 °C/min over a temperature range of 20–85 °C while monitoring its absorbance at 260 nm. The total variation in absorbance over all four runs was 0.0015 AU and after the first heating and cooling cycle it was 0.0010 AU. This was very similar to the performance of phosphate buffer (POB)-cryoprotectant in the same test. At the end of the four cycles of heating and cooling, the pH of the PIB-cryoprotectant was tested with pH paper and was found to lie between pH 6.8 and 7.1.

3.4. Circular dichroism (CD) and ultraviolet (UV) spectra

A-form, B-form, and Z-form DNA produce circular dichroism spectra that are characteristic of each form [28,29]. While the precise shape of the CD spectrum is also a function of DNA sequence, each form has a characteristic "signature." B-form DNA shows a positive rotation above ~260 nm and a negative rotation below. The CD spectrum of the native DNA duplex in PIB at 15 °C, Fig. 3(a), is characteristic of B-form DNA. The spectrum changes slightly when the cryoprotectants PEG 6000 and EG are added, most notably with a decrease in ellipticity in the positive CD band above 260 nm and a shift in the crossover point to longer wavelengths. Similar changes have been observed in duplex DNA with the addition of ethanol [15] or at high salt concentrations [30,31] and probably result from the decreased activity of water. A further decrease in the positive rotation above 260 nm and a further shift in the crossover point to longer wavelength are observed when the temperature decreases from 15 to −10 °C, Fig. 3(a). However, the CD spectra of the native duplex in PIB-cryoprotectant at these temperatures are still consistent with B-form DNA, possibly with a slight change in the number of bases per turn [32–34]. The CD spectra of the native duplex in POB and POB-cryoprotectant (data not shown) are very similar to those for PIB and PIB-cryoprotectant shown in Fig. 3(a).

The chemically modified DNA duplexes display CD spectra that are characteristic of B-form DNA and very similar to the native duplex. Fig. 3(b) shows the CD spectra collected in PIB-cryoprotectant. The CD spectrum of the SL-duplex overlaps that of the native duplex except between 260 and 300 nm where its positive band is slightly smaller. The CD spectrum of the SEDy-duplex deviates slightly from that of the native duplex in that its negative band is slightly smaller in magnitude, its positive band is greater in magnitude, and the peak of the positive band is shifted to shorter wavelengths. Most noticeably, its CD spectrum shows a new feature, a broad, shallow negative band from 295 to 350 nm. Although not shown here, the CD spectrum of the SECa-duplex is nearly identical in shape and intensity to that of the SEDy-duplex.

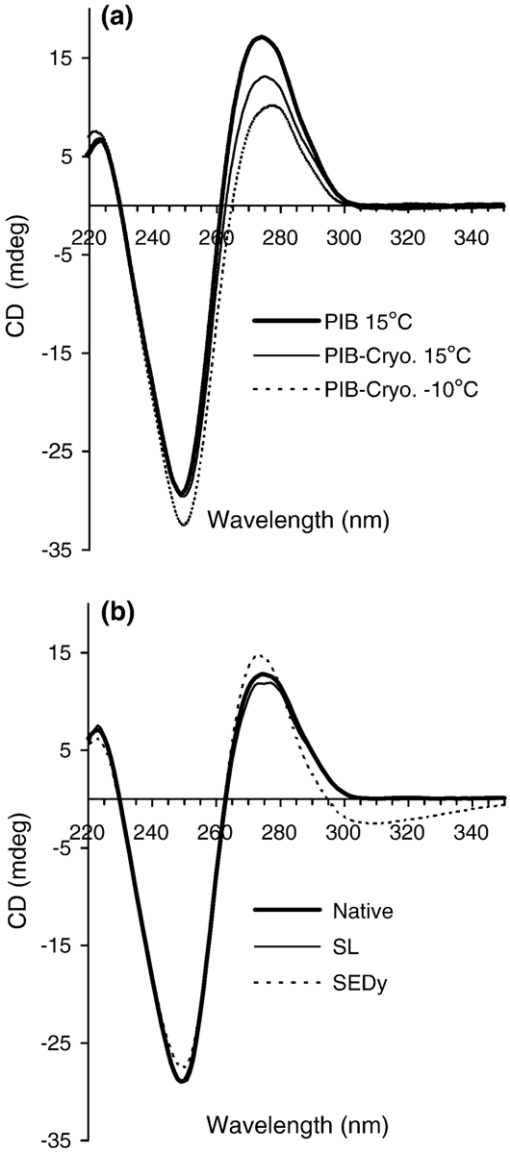

Fig. 3. (a) Circular dichroism spectra of the native duplex. (b) Circular dichroism spectra of the native and chemically modified DNA duplexes in PIB-cryoprotectant at 10 °C. The CD spectrum of the SECa-duplex (not shown) is essentially indistinguishable from that of the SEDy-duplex.

The UV spectra of these two DNA duplexes also share in common a weak, broad absorbance band above 300 nm that is not observed in the UV spectra of the native duplex or the SL-duplex, Fig. 4.

Since a CD band can only arise where there is absorption of light, the broad negative CD band between 295 nm and 350 nm observed in the CD spectra of the SEDy- and SECa-duplexes presumably arises from the broad absorbance band in the UV seen at the same wavelengths. Several experiments were performed to determine the source of these new features. UV spectra of EDTA(Dy(III)) and EDTA(Ca(II)) "free" in solution showed no detectable absorbance above 300 nm at these concentrations. Furthermore, when equimolar EDTA(Dy(III)) or HEDTA(Dy(III)) were added to the SL-duplex, no absorbance above 300 nm was observed and no broad negative rotational band was produced in the CD spectrum between 295 and 350 nm. These observations appear to rule out the EDTA-moiety of the EDTA-T19mer as the direct source of these features in the CD and absorbance spectra.

UV absorbance and CD spectra were collected as the SEDy-duplex was heated. It was observed that the circular dichroism of the band at 295–350 nm decreased approximately in parallel with the melting of the DNA duplex, as monitored by the absorbance at 260 nm. However, the UV absorbance band in the 300–350 nm range was present and essentially unchanged in intensity over the 10 to 70 °C temperature range, indicating that the structure producing the absorbance band was present even when the DNA duplex had completely melted. Finally, when the SE-duplex was prepared, both the UV absorbance above 300 nm and the broad negative band between 295 and 350 nm in the CD spectra were produced, even though the EDTA-moiety of the E-T19mer was presumably empty of multivalent cations. It was concluded from these experiments that both features arise from the modified base dT-EDTA but do not require the EDTA moiety itself. This modified base has a linkage that connects the pyrimidine base to the EDTA moiety. The portion closest to thymidine is composed of conjugated double bonds that apparently alter the ultraviolet absorption and circular dichroism of this chromophore, Fig. 1(b).

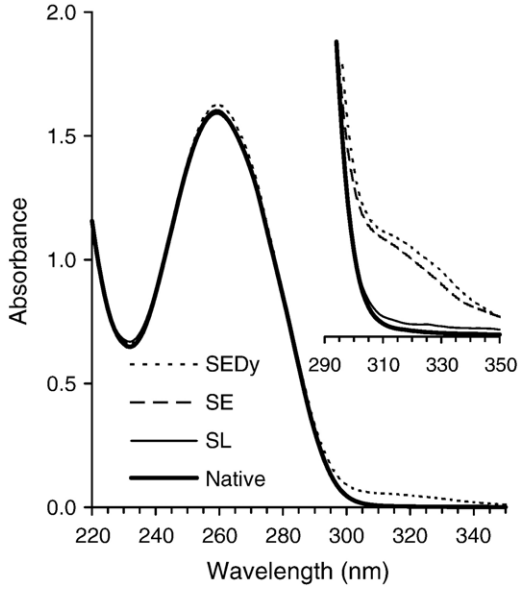

Fig. 4. Ultraviolet absorption spectra of DNA duplexes in PIB-cryoprotectant at 10 °C. The inset shows the spectra from 290 to 350 nm on an expanded vertical scale. For clarity, the absorption spectrum of the SE-duplex is shown only in the 290 to 350 nm region. The absorption spectrum of the SECa-duplex (not shown) is essentially indistinguishable from that of the SEDy-duplex.

3.5. Determination of thermodynamic parameters T_m and $\Delta H°$

Since the new CD band from dT-EDTA was well separated from the rest of the CD spectrum and it showed a cooperative change with melting, it became apparent that it could provide information on the local thermodynamic stability of the DNA duplex. The melting temperature, T_m and the enthalpy of melting, $\Delta H°$, can be calculated from changes in ellipticity or absorbance in a straightforward manner if one assumes a two-state model, that is, that each DNA strand is either in duplex form or single-stranded [35]. The two-state model is generally accepted for DNA oligonucleotides that are 12 base pairs in length or shorter. To determine whether the two-state model was applicable to the 19 base-pair native duplex, the enthalpy of duplex melting, $\Delta H°$, was determined from the absorbance change at 260 nm. This experimental value was then compared to $\Delta H°$ calculated from a nearest neighbor analysis, which can be done quite accurately regardless of the precise buffer conditions [36]. The experimentally determined $\Delta H°$ was 607 kJ/mol in PIB while the calculated value of $\Delta H°$ was 601 kJ/mol. The fact that these two values are within 1% of each other indicates that the two-state model accurately describes the melting of the native duplex.

Absorbance and circular dichroism spectra of the native duplex, SL-duplex, SEDy-duplex, and SECa-duplex in PIB-cryoprotectant were collected simultaneously in 1 °C increments over the temperature range 10–70 °C as described in the Experimental section. To monitor the global transition from duplex to single-stranded states, absorbance at 260 nm [35], $A_{260\ nm}$, and circular dichroism at 248 nm [37], $[\theta_{248\ nm}]$, were plotted versus temperature. To monitor the transition from duplex to single-stranded state in the vicinity of the dT-EDTA conjugate, circular dichroism at 310 nm, $[\theta_{310\ nm}]$, was plotted versus temperature. This wavelength was chosen to avoid contributions from bases other than dT-EDTA, while still being near the band's maximum (most negative) ellipticity. Fig. 5 shows normalized melting curves based on $A_{260\ nm}$ for the native duplex, SL-duplex, SEDy-duplex and SECa-duplex. Fig. 6 shows a melting curve based on $[\theta_{310\ nm}]$ for the SEDy-duplex.

Both the melting temperature, T_m, and the enthalpy change associated with melting, were calculated from the shape of the cooperative transitions as described by Marky and Breslauer [35]. The extent of duplex formation, α, was calculated as described in the legend to Fig. 6 and plotted against temperature. The melting temperature, T_m, was taken to be the temperature at $\alpha = 0.5$. The enthalpy of melting was then calculated from

$$\Delta H° = -6RT_m^2\left(\frac{d\alpha}{dT}\right)_{T_m} \quad (1)$$

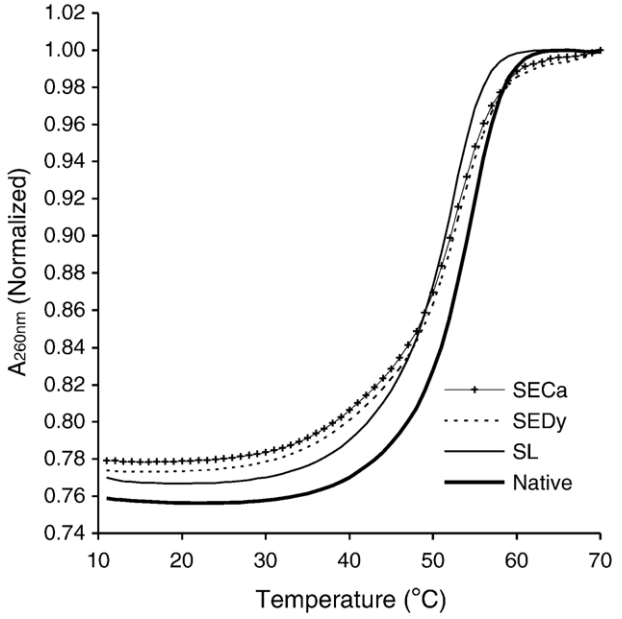

Fig. 5. UV-monitored melting curves for 4 DNA duplexes. The normalized absorbance at 260 nm is shown as a function of temperature.

where R is the universal gas constant and the slope at T_m in the curve α versus T yields the derivative in this equation.

The results of this analysis are shown in Tables 2 and 3 below. Table 2 lists the percent (%) hyperchromism and the changes in circular dichroism for each duplex where "Total" is the change over the entire 10–70 °C temperature range and "Melt" is the change observed during the cooperative transition. The percent hyperchromism was calculated as % Hyperchromism $= \Delta A_{260\ nm}/A^{max}_{260\ nm} \times 100$. The presence of dT-EDTA in the duplex and either Ca(II) or Dy(III) resulted in a small decrease in both the total hyperchromism and the hyperchromism during the cooperative transition. It also produced a slight decrease in the total change in circular dichroism at 248 nm, although in this case there may be a contribution from the spin-label also. These differences may indicate some perturbation of the DNA secondary structure. If so, it appears that it is a modest perturbation since all four duplexes exhibited the same change in circular dichroism at 248 nm during the cooperative transition. We also note that while the changes in circular dichroism at 310 nm were small, they were very reproducible, particularly during the cooperative transition.

The two monitors of global melting, $A_{260\ nm}$ and $[\theta_{248\ nm}]$, produced values for T_m and $\Delta H°$ that were very similar to each other for each duplex, Table 3. While the T_m and $\Delta H°$ values calculated from $[\theta_{310\ nm}]$ are very similar in the SEDy- and SECa-duplexes, they are higher than the corresponding values from $A_{260\ nm}$ and $[\theta_{248\ nm}]$. From Table 3, it may appear that for the SEDy-duplex the T_m values from $A_{260\ nm}$, $[\theta_{248\ nm}]$, and $[\theta_{310\ nm}]$ are within the uncertainty of each other. However, within each of the trials, the T_m determined from $[\theta_{310\ nm}]$ was higher than that determined from $A_{260\ nm}$ or $[\theta_{248\ nm}]$. Therefore, while modest, we believe that the difference in T_m values is real for both the SEDy- and SECa-duplexes. Overall the results in Table 2 indicate that the region of the helix near dT-EDTA is thermodynamically more stable in the SEDy- and SECa-duplexes than the rest of the helix and they suggest that presence of dT-EDTA with either Dy(III) or Ca(II) is responsible for this increased stability.

3.6. Dynamics of the spin-label

EPR spectroscopy was used to examine the dynamics of the spin-label in the DNA duplexes as a function of temperature in PIB-cryoprotectant. If the spin-label is free to diffuse at the end of its flexible tether to the DNA duplex, then it should have a correlation time only slightly longer than that of the free (untethered) spin-label. Conversely, if it is bound to the DNA duplex through hydrogen bonding or other interactions, then it should tumble with a much longer correlation time. Thus the correlation time is an inverse measure of the mobility of the spin-label. Shorter correlation times indicate greater mobility.

The EPR spectrum of a rapidly tumbling spin-label displays three lines due to hyperfine coupling between the electron spin and the ^{14}N (spin = 1) nucleus. An effective correlation time for the spin-label can be calculated from the relative heights and linewidths of the central and high field lines [38,39] using the equation

$$\tau(s) = 6.5 \times 10^{-10} \Delta H_0 \left(\sqrt{\frac{h(0)}{h(-1)} - 1} \right) \qquad (2)$$

where $h(0)$ and $h(-1)$ are the peak-to-peak heights of the central and high field lines, respectively, and ΔH_0 is the peak-to-peak width of the central line in the first-derivative EPR spectrum, Fig. 7.

The correlation times of the SL-, SECa-, SEDy-, and SE-duplexes and the free nitroxide (NO) spin-label, 1-Oxyl-2,2,5,5-tetramethylpyrroline-3-carboxylate, are plotted as a function of temperature over the range 0 °C ≤ T ≤ 30 °C in the inset to

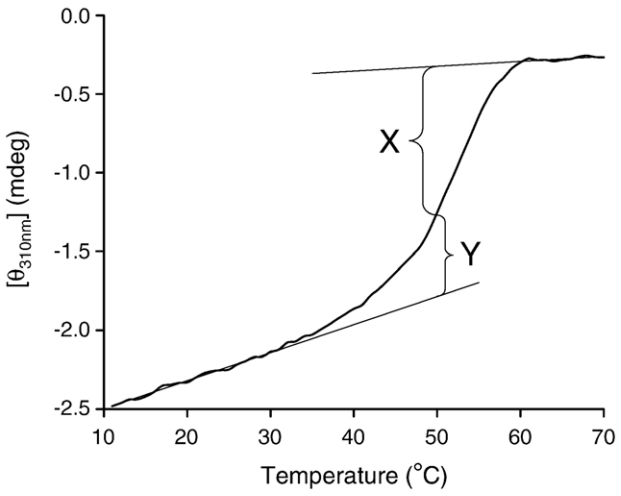

Fig. 6. CD-monitored melting curve for the SEDy-duplex. Circular dichroism at 310 nm is shown as a function of temperature. The straight lines are fits to the pre- and post-cooperative transition data and are used to calculate X and Y at each temperature within the cooperative transition region. These in turn were used to calculate the extent of reaction (duplex formation), α, where $\alpha = X/(X+Y)$.

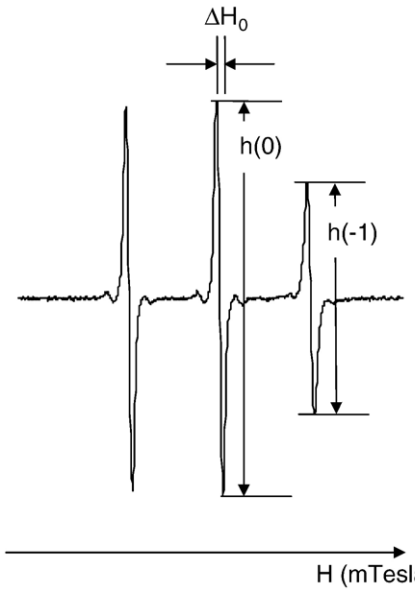

Fig. 7. Lineshape parameters in the EPR spectrum of a nitroxide radical used to determine its correlation time from Eq. (2).

Fig. 8. Decreasing the temperature of the solution increases its viscosity and, consequently, the correlation time, as illustrated by the behavior of the free spin-label. In all four DNA duplexes, the correlation time of the spin-label is increased by its covalent linkage to DNA, inset to Fig. 8, even though this linkage is presumably quite flexible, Fig. 1(a). However, one also observes that the correlation times of the spin-labels in the SECa- and the SEDy-duplexes are very similar to each other but significantly greater than those of the SL-duplex at each temperature. In contrast, the spin-label of the SE-duplex apparently has the same mobility as that of the SL-duplex. Thus, while Ca(II) or Dy(III) bound to the EDTA-moiety of dT-EDTA reduces the mobility of the spin-label, the presence of dT-EDTA alone does not. Furthermore, the presence of Dy(III) alone is not sufficient to inhibit the mobility of the spin-label. In a sample where one equivalent of Dy(III) was added to the SL-duplex, the correlation times of the spin-label were the same as those observed in the SL-duplex without added Dy(III) (data not shown).

Shorter correlation times are expected for the spin-label when its DNA strand goes from duplex to single-stranded forms [40,41]. Since the SL-, SECa-, and SEDy-duplexes all carry the same spin-labeled strand, that is, the SL-A19mer, the correlation times of the spin-label should converge to the same (shorter) value once melting of the duplexes is complete. Conversely, if complete melting occurs at a higher temperature for one duplex than for another, then the correlation times of the spin-label will not converge to a common value until the higher temperature is reached.

An experiment was conducted in which EPR spectra of these three duplexes were collected at 3 °C increments over the temperature range from 30 to 69 °C. Correlation times were then calculated as described earlier and are shown plotted in Fig. 8 as a function of temperature. The correlation times of the spin-label in the SL-duplex reach a limiting value of 0.42 ± 0.02 ns by 63 °C, indicating that melting is complete by this temperature. In contrast, the correlation times of the spin-labels in the SECa- and SEDy-duplexes are still significantly longer than those of the SL-duplex at 63 °C. Convergence of the three correlation times does not occur until 69 °C. This is consistent with the spin-labeled termini of the SECa- and SEDy-duplexes melting later than that of the SL-duplex. These results are in rough agreement with the UV-monitored melting curves shown in Fig. 5 which show that melting is complete by ~60 °C for the SL-duplex while melting is not complete until ~69 °C for the SECa- and SEDy-duplexes. (Note that for the SL-duplex, the correlation times at 60 and 63 °C are equal within the uncertainty, Fig. 8.) It is also noteworthy that the correlation times of the spin-labels in the SECa- and SEDy-duplexes are within the error of each other throughout this temperature range, indicating that the melting behavior of these two duplexes is very similar.

3.7. Microwave progressive power saturation

In a continuous-wave EPR experiment, a signal is observed by continuous irradiation of the sample at the appropriate frequency and magnetic field. A signal can be observed because at equilibrium, the population of the lower energy spin-state, “spin down” is greater than that of the higher energy spin state, “spin up” and so there is a net absorption of microwave energy. If the microwave energy used to observe the unpaired electron spins is of low intensity, then the observation does not perturb the equilibrium populations of the two spin states because

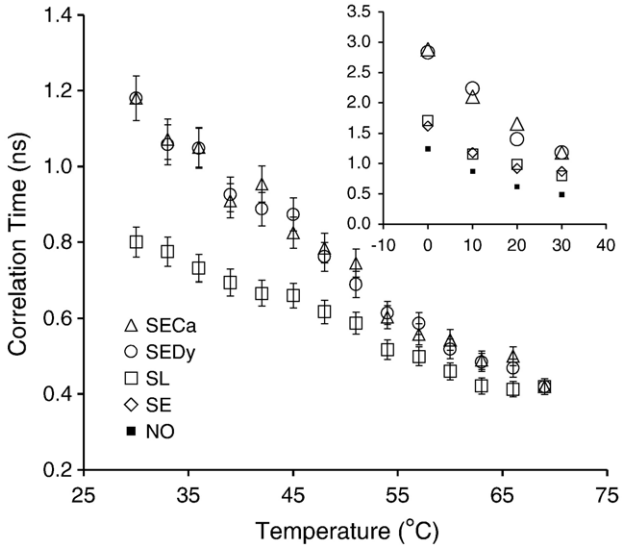

Fig. 8. Inset: correlation times calculated from CW EPR spectra and Eq. (2) for the SECa-, SEDy-, SL- and SE-duplexes and the corresponding “free” spin-label. The temperature dependence of the correlation time for the “free” spin-label shows the effect of solvent viscosity. The height of the symbols is approximately equal to the standard deviation in the measurements. Main figure: correlation times calculated from CW EPR spectra and Eq. (1) for the SECa-, SEDy-, and SL-duplexes. The onset of melting in these three duplexes is approximately 30 °C, based on the melting curves shown in Fig. 5. The error bars indicate the uncertainty in the correlation times.

transitions between the two states occur fast enough to maintain this equilibrium. As the microwave power increases, the populations of the two spin states are perturbed such that the population of spins in the higher energy state approaches that in the lower energy state and the EPR signal is described as partially saturated. Complete saturation of a signal, although not typically realized in practice, results if the microwave power is sufficiently high that the two spin-states are equally populated. In this case, no absorption of microwave energy is observed.

An equation that describes this microwave progressive power saturation experiment, derived from the work of Portis [42] and Castner [43], is shown below. In Eq. (3), S' is the peak-to-peak height of the first derivative signal, K is a constant, P is the microwave power, $P_{1/2}$ is the power at half saturation, and b is a parameter describing the type of line broadening present in the EPR signal, with a value of 1 being the limit for inhomogeneous line broadening and a value of 3 being the limit for purely homogeneous line broadening.

$$S' = \frac{K\sqrt{P}}{\left(1 + P/P_{1/2}\right)^{b/2}} \tag{3}$$

In purely homogeneous broadening, (b=3), the width of the signal reflects the intrinsic linewidth, k_2/π, where k_2 is the spin–spin (spin dephasing) relaxation rate. For the case of inhomogeneous broadening, (b=1), the linewidth represented by k_2/π is insignificant compared to the observed signal, which is essentially an envelope that encompasses spins (radicals) resonating at a wide range of frequencies (fields) because of anisotropy in the g-tensor or hyperfine couplings. For radicals in a frozen solution or glass, it is typical for the line broadening to be primarily inhomogeneous in nature.

Eq. (3) indicates that when the EPR signal is not saturated, that is, at low microwave observe powers where $P/P_{1/2} << 1$, the EPR signal amplitude increases linearly with the square root of the observe microwave power. In this low microwave observe power limit, division of the signal amplitude by the square root of the observe power, $S'/\sqrt{P}$, gives a constant value equal to K. The degree of saturation in two different samples can be compared by normalizing their respective signals, that is, by plotting $S'/\left(K\sqrt{P}\right)$ versus P. It is conventional to take the logarithm of both sides of Eq. (3) or to plot the data on a log–log plot because this produces two linear regions.

$$\log\left(\frac{S'}{K\sqrt{P}}\right) = -\frac{b}{2}\log\left(1 + \frac{P}{P_{1/2}}\right) \tag{4}$$

At low power, $P/P_{1/2} << 1$, the data points produce a horizontal line, since in this regime $S'/\left(K\sqrt{P}\right) = 1$, and at high power, $P/P_{1/2} >> 1$, the data points produce a straight line with a slope of $-b/2$, Fig. 9. These two lines intersect at $P_{1/2}$.

The microwave power at half saturation, $P_{1/2}$, is proportional to the product of the spin-lattice and spin–spin relaxation rates, k_1 and k_2, of the observed radical [44]. The faster these rates, the greater $P_{1/2}$, and the smaller the degree of saturation for a given level of microwave power, that is, the closer $S'/\left(K\sqrt{P}\right)$ will be to 1, the non-saturating constant value. For a

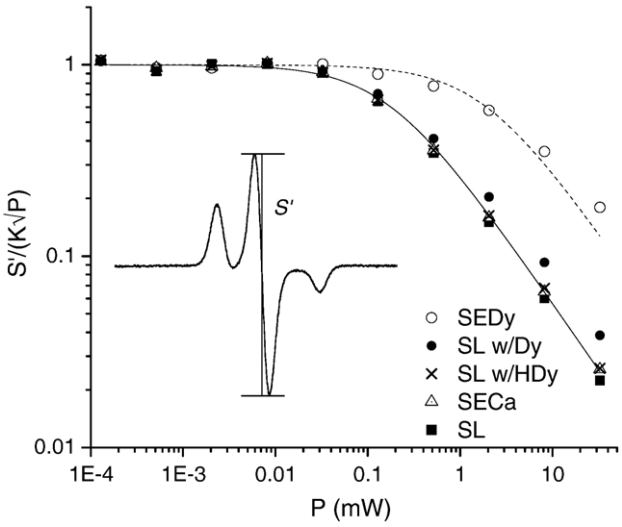

Fig. 9. Microwave progressive power saturation results. The inset shows how the first derivative signal amplitude, S', was measured. For each sample, K was calculated by taking the average value of $S'/\sqrt{P}$ for the spectra collected at the four lowest levels of microwave power. The error in these measurements is equal to the height of the symbols, based on experimental measurements repeated on separate days. All EPR spectra were collected at 77 K using 3.2 G field modulation.

radical species, spin-lattice and spin–spin relaxation rates can be enhanced by the presence of a nearby paramagnetic metal ion by means of dipole–dipole (through space) or exchange (through bond) interactions [1,2]. Therefore, in the presence of a nearby paramagnetic metal ion, $P_{1/2}$ will be greater for a radical and *more* microwave power will be required to achieve the same level of saturation. The expectation then is that the spin-label in the SEDy-duplex should require more microwave power to achieve a given level of saturation than the spin-label in the SL- or SECa-duplexes because of the proximity of paramagnetic Dy(III) to the nitroxide spin-label in the SEDy-duplex. Simple model building indicates that if the DNA duplex adopts a B-form conformation, the spin-label and the Dy(III) ion will be within approximately 19 Å each other.

Fig. 9 compares the saturation behavior of the spin-label in the SL-, SECa-, and SEDy-duplexes and in two control samples at 77 K. From the "high power" data on the right hand side of the plot, it is clear that the spin-label in the SEDy-duplex requires more power than the spin-label in the SL- and SECa-duplexes to achieve the same level of saturation, which is consistent with the presence of a nearby paramagnetic metal ion. Also consistent with expectations, the saturation curves for the spin-labels in the SL- and SECa-duplexes are very similar.

Data from the two control samples support the hypothesis that the Dy(III) ions are bound by the EDTA moiety of dT-EDTA. In the control samples, equimolar Dy(III) was added to a solution of SL-duplex in the form of either HEDTA(Dy(III)), indicated as "SL w/HDy" or $DyCl_3$, indicated as "SL w/Dy." As seen in Fig. 9, addition of HEDTA(Dy(III)) to the SL-duplex has a negligible effect on the spin-label's saturation behavior. This is expected if the metal complex remains dispersed in solution or if it can only bind to the DNA duplex at sites distant from the spin-

label. The addition of $DyCl_3$ to the SL-duplex does have a measurable effect on the saturation behavior of the spin-label. This is not surprising since the condensation of divalent and trivalent cations on DNA is well known [45]. Even so, the spin-label in the SEDy-duplex requires approximately an order of magnitude more power to achieve the same level of saturation as the spin-label in the SL-duplex with added $DyCl_3$.

The solid line in Fig. 9 is a fit of the microwave power saturation data for the spin-label in the SECa-duplex to Eq. (4), where both b and $P_{1/2}$ were adjustable parameters. The data are well fit when $b=1.4$, indicating that there are both homogeneous and inhomogeneous contributions to the linewidth. Relaxation enhancement can only *increase* the value of b by making k_2 faster and hence, the homogeneous component of the linewidth, k_2/π, greater. When the data from the microwave progressive power saturation of the spin-label in the SEDy-duplex are fit to Eq. (4), (broken line), the data are not well fit when b is fixed at 1.4. Furthermore, the fit can only be improved by *decreasing* the value of b. The best fit value for b is found to be 0.8, which is below the limit of 1 for inhomogeneous broadening.

This behavior is characteristic of relaxation enhancement via a dipole–dipole interaction [46]. The relaxation enhancement caused by dipole–dipole interactions is orientation dependent, that is, the degree to which the dipole–dipole interaction enhances the overall rate constants k_1 or k_2 depends on the angle formed by the magnetic field vector and the vector that connects the two paramagnetic sites (metal ion and radical). For a sample that consists of a frozen solution or suspension, all orientations are present and so, within a single sample, there can be a wide variation in k_1 or k_2 and therefore in $P_{1/2}$. This range of $P_{1/2}$ values causes the saturation curve to be "stretched" along the x-axis. The result is that the apparent value of b decreases when a dipole–dipole interaction is a significant source of relaxation enhancement [6]. Work in proteins indicates that the dipole–dipole interaction is a more significant source of relaxation enhancement than the exchange interaction for distances greater than ~10 Å between a radical and a paramagnetic metal site [7]. If the distance dependence of exchange interactions is similar in DNA, then these results indicate a distance greater than 10 Å between the Dy(III) ion and the spin-label in the SEDy-duplex.

4. Discussion

4.1. Buffer-cryoprotectant glass

We have developed a buffer-cryoprotectant solution, PIB/PEG 6000/EG, 55/30/25, w/w/w, that preserves the B-form conformation of DNA and does not complex metal ions. The small temperature coefficient and glass-forming properties of this buffer system will permit low-temperature EPR, room temperature optical, and low-temperature optical spectroscopy experiments to be carried out on the same sample.

Low-temperature (77 K) optical measurements on DNA have been made in an aqueous glass of 10 M LiCl [47]. However, high-salt solutions of this type are problematic for EPR. While a frozen glass of 10 M LiCl can probably be tuned inside an EPR cavity, an aqueous solution of 10 M LiCl almost certainly cannot, owing to its high conductance. For these experiments we wanted to be able to make EPR measurements in the same aqueous medium at both near-ambient and cryogenic temperatures. We therefore investigated the use of polyethylene glycol (polyethylene oxide) and ethylene glycol in forming aqueous glasses, encouraged by the observations of Spink and Chaires [48] that while the presence of ethylene glycol lowers the melting temperature of duplex DNA, due to dehydration of the DNA backbone, the presence of high molecular weight polyethylene glycols raises the melting temperature, due to volume exclusion effects.

We were surprised then that T_m was lower in the two-component solution containing only PEG 6000 than it was in the three-component solution containing both PEG 6000 and EG. However, it is reasonable since the highest weight percent of PEG tested by Spink and Chaires [48] was 20% whereas in the two-component and three-component cryoprotectant solutions described here, the weight percent of PEG was 50% and 30%, respectively. At these concentrations, excluded volume effects may play a role in depressing T_m. In dilute solution, the radius of gyration of PEG 6000 has been determined to be 32.7 Å. [49] Based on the total volume of the three-component solution used here, PEG 6000 has a significantly smaller radius of gyration (~20 Å) and/or significant interpenetration of the polymer coils. Since the DNA double helix is a relatively rigid polymer, the single stranded form of DNA might accommodate the PEG polymer better, favoring the formation of single-stranded DNA at a lower temperature and hence lowering T_m.

4.2. Circular dichroism (CD) and ultraviolet (UV) spectra

The modified base dT-EDTA chelates the metal ion in the SEDy- and SECa-duplexes and also provides a spectroscopic probe of local DNA melting because it has an absorbance and CD band that are red-shifted from those of unmodified DNA bases. The data are consistent with these features arising from electronic coupling between the conjugated π-orbitals in the linker and the pyrimidine ring of the deoxythymidine (deoxyuracil) moiety, rather than from the EDTA moiety or the EDTA moiety's interactions with the DNA duplex. We note that there are other commercially available deoxythymidine analogs, designed for covalent modification after oligonucleotide synthesis, that have the same conjugation [50] or that will yield the same conjugation upon amide bond formation [51]. When incorporated into DNA oligonucleotides, these dT-X conjugates should show features in the UV and CD spectra that are similar to those of dT-EDTA.

4.3. T_m and enthalpy of melting

For each of the four duplexes, the melting temperatures, T_m, determined from $A_{260\ nm}$ and $[\theta_{248\ nm}]$ are equal within the uncertainty and the $\Delta H°$ values determined from $A_{260\ nm}$ and $[\theta_{248\ nm}]$ are within 5% of each other, suggesting that these two spectroscopic measurements monitor the same melting transition

within each DNA duplex, Table 2. For the native duplex and the SL-duplex it seems reasonable to assume that melting can be described as a two-state process in PIB-cryoprotectant. This assumption is based on the following observations; melting of the native duplex is a two-state process in purely aqueous buffer (PIB), the melting curves based on $A_{260\ nm}$ and $[\theta_{248\ nm}]$ in PIB-cryoprotectant give no indication of intermediary states, and the two duplexes show similar melting temperatures and melting enthalpies. The values of $\Delta H°$ measured in PIB-cryoprotectant (~390 kJ/mol) are much lower than those calculated for and experimentally measured in purely aqueous buffer (~600 kJ/mol). They are consistent, however, with the decrease in T_m noted earlier in going from buffer to buffer-cryoprotectant and with the observation by Spink et al. [52] that EG and PEG decrease the enthalpy of melting in model DNA duplexes. While the decrease in enthalpy observed by Spink et al. [52] was quite modest, the highest concentrations of EG or PEG examined in their work (20% w/w) were significantly lower than the total cryoprotectant concentration used to make our PIB-cryoprotectant solution (45% w/w, cryoprotectant/buffer). It seems reasonable that the cryoprotectant concentration used here causes some additional dehydration of DNA that further lowers the enthalpy of melting.

For the SEDy- and SECa-duplexes, it appears that the two-state model may not be appropriate since the melting temperatures and transition enthalpies determined from the circular dichroism at 310 nm, while very similar in the two duplexes, are greater than those determined using $A_{260\ nm}$ and $[\theta_{248\ nm}]$. We suggest instead the three-state model shown schematically in Fig. 10. In this model, the T_m and $\Delta H°$ values determined from $A_{260\ nm}$ and $[\theta_{248\ nm}]$ reflect the melting of ~14 base pairs outside the region flanked by dT-EDTA and the spin-label, while the T_m and $\Delta H°$ values determined from $[\theta_{310\ nm}]$ reflect the complete melting of the DNA duplex. The T_m and $\Delta H°$ values determined for the SEDy- or SECa-duplexes are not quantitative measures of the melting transitions, but provide a qualitative description of the melting process in these two duplexes. Calorimetric measurements would be required to define this model unambiguously [35].

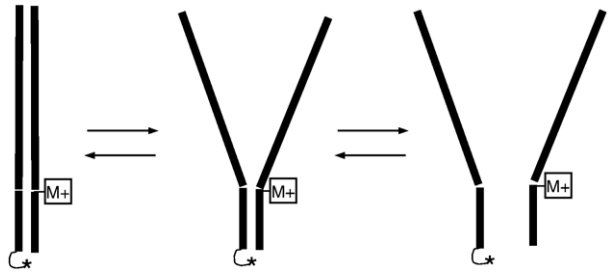

Fig. 10. A three state model for the melting of the SEDy- and SECa-duplexes. The asterisk (*) at the terminus of the left-hand DNA strand represents the nitroxide spin-label. The box (□) on the right-hand DNA strand represents dT-EDTA. M+ represents the bound metal ion, either Dy(III) or Ca(II). The first transition is the melting of the 14 base pairs above dT-EDTA in the duplex. The second transition is the melting of the remaining 5 base pairs flanked by dT-EDTA and the spin-label. Because T_m is similar for the two transitions, all three species can exist at significant concentrations at the same time.

Additional evidence that the base pairs lying between the spin-label and dT-EDTA melt later than the rest of the helix comes from the rotational correlation times determined from the CW EPR lineshape of the spin-label in the SL-, SEDy-, and SECa-duplexes. Correlation times measured over the 30 to 69 °C temperature range indicate that the base pairs flanked by the dT-EDTA and spin-labeled moieties are more resistant to melting. For the SL-duplex, the rotational correlation times reach a limiting value of 0.42 ns by 63 °C, indicating complete melting of the duplex by this temperature. On the other hand, the SEDy- and SECa-duplexes do not reach the same correlation time until 69 °C. That the longer correlation times for the spin label in the SEDy- and SECa-duplexes at these temperatures reflects differences in DNA base-pair melting is supported by the UV-monitored melting curves which indicate that melting is not complete for the SEDy- and SECa-duplexes until approximately 69 °C, Fig. 5. These temperatures are significantly higher than the T_m values determined from $A_{260\ nm}$, $[\theta_{248\ nm}]$, or $[\theta_{310\ nm}]$. This is expected, however, since T_m values indicate the temperature at which half the DNA is in duplex form. In this experiment, the temperature at which melting is complete is measured.

The data support a one-to-one pairing of added Ca(II) or Dy(III) and the EDTA moiety of dT-EDTA and a single conformation for the spin-labeled termini of the SECa- and SEDy-duplexes. First, the change in ellipticity at 310 nm with temperature is identical in the two duplexes and highly reproducible, Table 3. Second, the similarity in spin-label correlation times between the SECa- and SEDy-duplexes over the entire temperature range suggest that the changes induced by metal-ion binding at dT-EDTA are consistent and homogeneous, Fig. 8. Thirdly, the microwave progressive power saturation experiments indicate that the binding of Dy(III) in the SEDy-duplex is specific since it requires much more power to reach the same level of saturation in this sample as compared to the SL-duplex with added Dy(III), Fig. 9.

What is yet uncertain is why the correlation times for the nitroxide spin-label differ in the different DNA duplexes. From 0 to 30 °C, the correlation times of the spin-labels in the SEDy- and SECa-duplexes are equal to each other or nearly so and yet are significantly longer than those of the SL- and SE-duplexes, Fig. 8, inset. It seems unlikely that the reduced mobility of the spin-label in the SECa- or SEDy-duplexes is the result of a direct contact between the EDTA(metal ion) chelate and the spin-label. Model building with the DNA duplex in the B-form conformation indicates that direct interaction of the two moieties would require full extension of the two tethers and a number of energetically unfavorable contacts. In addition, contact between the EDTA moiety and the spin label would result in a distance of only a few Ångstroms between Dy(III) and the nitroxide radical, which is not consistent with the microwave progressive power saturation experiment, Fig. 9. If there were contact between the EDTA(Dy(III)) complex and the nitroxide spin-label, the exchange interaction would be the dominant mechanism for enhancing k_1, k_2 and, therefore, $P_{1/2}$. Since the exchange interaction is not orientation dependent, the parameter b would be expected to either remain constant or increase.

In studies by Bobst and coworkers, changes in DNA conformation from B to Z-form could be detected by EPR using spin-labels with long (11-atom) tethers to a cytidine analog [41,53]. The EPR signals reported by Bobst and coworkers have lineshapes comparable to those observed here, suggesting that the correlation times that would be calculated from Eq. (2) would also be comparable. Their cytidine-tethered spin-label showed a longer correlation time when the DNA was in the Z-form than when it was B-form. This was interpreted to mean that base dynamics in the DNA duplex were slower and/or smaller in amplitude in the Z-form.

In the duplexes described here, the nitroxide spin-label is covalently linked to the deoxyribose/phosphodiester backbone of the SL-A19mer via a 5-atom chain, Fig. 1(b). We note that crystallographic data indicates that the mobility of the phosphate and ribose groups is even greater than that of the bases and that there is also evidence that the terminal nucleosides may experience larger amplitude motions than those near the center of the helix [54–56]. We suggest that in the SEDy- and SECa-duplexes, the EDTA-metal ion chelate complexes with the backbone of DNA in such a way as to reduce the amplitude and/or frequency of librational motions in the DNA backbone and that this results in an increase in the correlation time of the terminal spin-label.

One possible way to test this hypothesis is to complex different metal ions with dT-EDTA. Calcium and dysprosium ions share in common an affinity for "hard" ligands that contain oxygen. If the Dy(III) or Ca(II) ions in dT-EDTA(Dy(III)) or dT-EDTA(Ca(II)) coordinate directly to the phosphates in the DNA backbone, then the substitution of transition metal ions that prefer "soft" ligands, like Zn(II) or Co(II), may result in weaker coordination to the DNA backbone, coordination to the nitrogenous bases, or no coordination at all. Any of these changes should result in less restriction on the motion of the DNA backbone and hence shorter correlation times for the spin-label in the DNA duplex.

Unlike the situation of Bobst and coworkers where changes in the correlation time reflected changes in the DNA conformation, coordination of the EDTA-metal ion complex to the DNA backbone probably results in little or no perturbation to the B-form secondary structure. It appears more likely that the unusual features in the CD spectra of the SECa- and SEDy-duplexes arise primarily, if not solely, from the unusual circular dichroism of dT-EDTA. First, we note that the base sequence of the model duplex was designed to adopt a canonical B-form secondary structure and that even when the native duplex was suspended in either 80% ethanol or 4 M NaCl, there was no evidence of A-form or Z-form DNA in the CD spectra, (data not shown). Second, while we have noted differences between the CD spectra of the SECa- and SEDy-duplexes and those of the native duplex and SL-duplex, overall the CD spectra are still characteristic of B-form DNA. Given this observation, it seems reasonable to assume that the majority of the base pairs in the SECa- or SEDy-duplexes are in a B-form secondary structure and that any perturbation is localized to approximately the last 5 base pairs at the spin-labeled termini of these duplexes. In this case, it should be possible to reveal the conformation of these 5 base pairs by subtracting the appropriately weighted CD spectrum of the SL-duplex from that of the SECa- or SEDy-duplex. Fig. 11 shows the residual CD spectrum when the CD spectrum of the SL-duplex is multiplied by 14/19 and subtracted from that of the SEDy-duplex. The significant negative rotation at ~248 nm in the residual CD spectrum is not consistent with either A-form [15,57,58] or Z-form [29] DNA but rather suggests that these terminal base pairs also adopt a B-form secondary structure. Changing the scaling factor to 15/19 does not significantly alter the residual CD spectrum's appearance, Fig. 11.

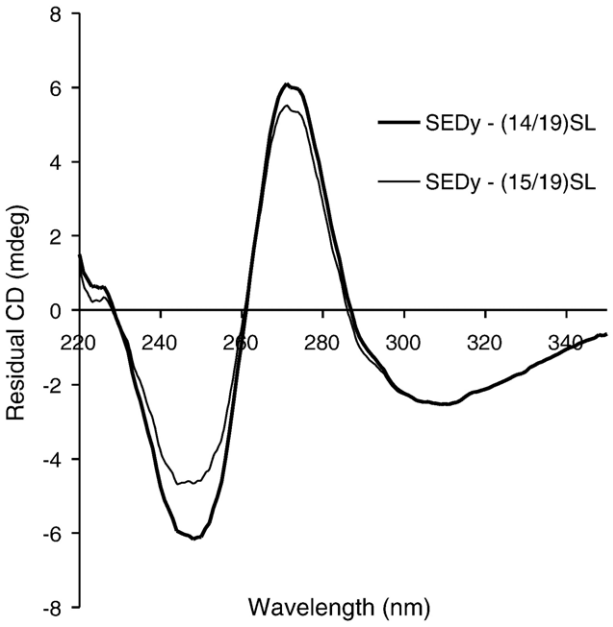

Fig. 11. The residual circular dichroism when the CD spectrum of the SL-duplex is subtracted from that of the SEDy-duplex. The two traces show the residual circular dichroism when the CD spectrum from the SL-duplex is first weighted by 14/19 (thick line) and 15/19 (thin line) prior to subtraction.

5. Conclusion

Our experimental results indicate that this DNA-based model system will be suitable for studying the electron spin–spin interactions between a variety of metal ions and the nitroxide radical. The CD spectra show that the conformation and thermodynamic properties of the model system are very similar when either Ca(II) or Dy(III) is bound by dT-EDTA. The microwave progressive power saturation experiment indicates that binding of Dy(III) is specific. Correlation times of the spin-label are essentially identical in the presence of chelated Ca(II) or Dy(III) and longer than they are in the absence of metal ions and/or dT-EDTA. The longer correlation times and the observed changes in DNA melting in the presence of chelated Ca(II) or Dy(III) suggest a specific interaction between the EDTA-metal ion complex and the DNA duplex. The mechanism by which the EDTA-metal ion complex affects the thermodynamic properties of the duplex and the mobility of the spin-label will be further investigated by introducing different metal ions into the model system and by varying the distance between the dT-EDTA and

the terminal spin-label. Future saturation-recovery EPR experiments will probe the spin-lattice (T_1) and spin–spin relaxation (T_2) behavior of paramagnetic metal ions by observing their effect on the spin-lattice relaxation of the nitroxide spin-label.

Acknowledgements

This research was supported by the American Chemical Society Petroleum Research Fund, Grant 41380-GB4, and The College of New Jersey. Xi Jun Chen and Heather Skiff were supported by summer research fellowships from National Starch & Chemical Co. Joseph Schramm was supported by a summer research fellowship from the Merck SURF 2004 program.

The authors would like to thank the following: Professor Gary W. Brudvig and the Department of Chemistry at Yale University for the generous donation of the Bruker/IBM ER200D ESR spectrometer used in these experiments, Professor Kathleen P. Howard of Swarthmore College for the use of her CW EPR instrument to determine the spin-label/A19mer ratio, and Dr. Alexei Tyryshkin of Princeton University for technical assistance in the early stages of this work.

References

[1] K. Lakshmi, G. Brudvig, Pulsed electron paramagnetic resonance methods for macromolecular structure determination, Curr. Opin. Struct. Biol. 11 (2003) 523–531.
[2] S.S. Eaton, G.R. Eaton, in: L.J. Berliner, G.R. Eaton, S.S. Eaton (Eds.), Distance Measurements in Biological Systems by EPR, Biological Magnetic Resonance, Kluwer Academic/Plenum Publisher, New York, 2000, pp. 348–378.
[3] V.J. DeRose, Metal ion binding to catalytic RNA molecules, Curr. Opin. Struct. Biol. 13 (2003) 317–324.
[4] Y. Zhou, B. Bowler, K. Lynch, S. Eaton, G. Eaton, Interspin distances in spin-labeled metmyoglobin variants determined by saturation recovery EPR, Biophys. J. 79 (2000) 1039–1052.
[5] G.R. Eaton, S.S. Eaton, in: L.J. Berliner, G.R. Eaton, S.S. Eaton (Eds.), Distance Measurements in Biological Systems by EPR, Biological Magnetic Resonance, Kluwer Academic/Plenum Publisher, New York, 2000, pp. 29–154.
[6] D.J. Hirsh, W.F. Beck, J.B. Innes, G.W. Brudvig, Using saturation-recovery EPR to measure distances in proteins: applications to photosystem II, Biochemistry 31 (1992) 532–541.
[7] D.J. Hirsh, W.F. Beck, J.B. Lynch, L. Que, G.W. Brudvig, Using saturation-recovery EPR to measure exchange couplings in proteins: application to ribonucleotide reductase, J. Am. Chem. Soc. 114 (1992) 7475–7481.
[8] D. Koulougliotis, D.J. Hirsh, G.W. Brudvig, The O_2-evolving center of photosystem II is diamagnetic in the S1-resting state, J. Am. Chem. Soc. 114 (1992) 8322–8323.
[9] D.J. Hirsh, G.W. Brudvig, Long-range electron spin–spin interactions in the bacterial photosynthetic reaction center, J. Phys. Chem. 97 (1993) 13216–13222.
[10] J. Burchfield, J. Du, K. More, M. Kundalika, S. Eaton, G. Eaton, Enhancement of electron spin relaxation rates of metalloporphyrins due to interaction with a faster relaxing metal bound to an appended bipyridyl, Inorg. Chim. Acta 263 (1997) 23–33.
[11] M. Rakowsky, K. More, A. Kulikov, G. Eaton, S. Eaton, Time-domain electron paramagnetic resonance as a probe of electron-electron spin–spin interaction in spin-labeled low-spin iron porphyrins, J. Am. Chem. Soc. 117 (1995) 2049–2057.
[12] R. Konda, J. Du, S. Eaton, G. Eaton, Electron spin relaxation rates for nitridochromium(V) tetratolylporphyrin and nitridochromium(V) octaethylporphyrin in frozen solution, Appl. Magn. Reson. 7 (1994) 185–193.
[13] J. Du, G. Eaton, S. Eaton, Electron spin relaxation in vanadyl, copper(II), and silver(II) porphyrins in glassy solvents and doped solids, J. Magn. Reson., Ser. A 119 (1996) 240–246.
[14] M. Seiter, V. Budker, J.-L. Du, G.R. Eaton, S.S. Eaton, Interspin distances determined by time domain EPR of spin-labeled high-spin methemoglobin, Inorg. Chim. Acta 273 (1998) 354–366.
[15] D.M. Gray, R.L. Ratliff, M.R. Vaughan, Circular dichroism spectroscopy of DNA, Methods Enzymol. 211 (1992) 389–406.
[16] Glen Research, EDTA-C2-dT-CE Phosphoramidite, 10-1059-xx, 03/11/2007, http://www.glenres.com/.
[17] G. Kallansrud, B. Ward, A comparison of measured and calculated single- and double-stranded oligodeoxynucleotide extinction coefficients, Anal. Biochem. 236 (1996) 134–138.
[18] R.G. Kooser, E. Kirchmann, T. Matkov, Measurements of spin concentration in electron paramagnetic resonance spectroscopy: preparation of standard solutions from optical absorption, Concepts Magn. Reson. 4 (1992) 145–152.
[19] D. Barr, J. Jiang, R.T. Weber, How to quantitate nitroxide spin adducts using tempol, EPR application notes, Bruker Biospin, 2005, http://www.bruker-biospin.com/documentation_epr.html.
[20] V. Nagy, Quantitative EPR: some of the most difficult problems, Appl. Magn. Reson. 6 (1994) 259–285.
[21] J. Jang, How to optimize EPR parameters for spin adducts, EPR Application Notes, EPR Division of Bruker Biospin, 2005, http://www.bruker-biospin.com/documentation_epr.html.
[22] J.B. Innes, G.W. Brudvig, Location and magnetic relaxation properties of the stable tyrosine radical in photosystem II, Biochemistry 28 (1989) 1116–1125.
[23] T. Sarna, J. Hyde, H. Swartz, Ion-exchange in melanin: an electron spin resonance study with lanthanide probes, Science 192 (1976) 1132–1134.
[24] J.E. Lovelock, The denaturation of lipid-protein complexes as a cause of damage by freezing, Proc. R. Soc. Lond., B Biol. Sci. 147 (1957) 427–433.
[25] D.D. Perrin, B. Dempsey, Buffers for pH and Metal Ion Control, Chapman and Hall, London, 1979.
[26] N.E. Good, G.D. Winget, W. Winter, T.N. Connolly, S. Izawa, R.M. Singh, Hydrogen ion buffers for biological research, Biochemistry 5 (1966) 467–477.
[27] J.S. Blanchard, Buffers for enzymes, Methods Enzymol. 104 (1984) 404–414.
[28] M.J. Tunis-Schneider, M.F. Maestre, Circular dichroism spectra of oriented and unoriented deoxyribonucleic acid films—a preliminary study, J. Mol. Biol. 52 (1970) 521–541.
[29] F.M. Pohl, T.M. Jovin, Salt-induced co-operative conformational change of a synthetic DNA: equilibrium and kinetic studies with poly (dG-dC), J. Mol. Biol. 67 (1972) 375–396.
[30] V.I. Ivanov, L.E. Minchenkova, A.K. Schyolkina, A.I. Poletayev, Different conformations of double-stranded nucleic acid in solution as revealed by circular dichroism, Biopolymers 12 (1973) 89–110.
[31] C.A. Sprecher, W.A. Baase, W.C. Johnson, Conformation and circular dichroism of DNA, Biopolymers 18 (1979) 1009–1019.
[32] W.A. Baase, W.C. Johnson Jr., Circular dichroism and DNA secondary structure, Nucleic Acids Res. 6 (1979) 797–814.
[33] C.Y. Chen, B.H. Pheiffer, S.B. Zimmerman, S. Hanlon, Conformational characteristics of deoxyribonucleic acid-butylamine complexes with C-type circular dichroism spectra. 1. An X-ray fiber diffraction study, Biochemistry 22 (1983) 4746–4751.
[34] C.H. Lee, H. Mizusawa, T. Kakefuda, Unwinding of double-stranded DNA helix by dehydration, Proc. Natl. Acad. Sci. U. S. A. 78 (1981) 2838–2842.
[35] L.A. Marky, K.J. Breslauer, Calculating thermodynamic data for transitions of any molecularity from equilibrium melting curves, Biopolymers 26 (1987) 1601–1620.
[36] J. SantaLucia Jr., A unified view of polymer, dumbbell, and oligonucleotide DNA nearest-neighbor thermodynamics, Proc. Natl. Acad. Sci. U. S. A. 95 (1998) 1460–1465.
[37] S.S. Chan, K.J. Breslauer, M.E. Hogan, D.J. Kessler, R.H. Austin, J. Ojemann, J.M. Passner, N.C. Wiles, Physical studies of DNA premelting

equilibria in duplexes with and without homo dA.dT tracts: correlations with DNA bending, Biochemistry 29 (1990) 6161–6171.
[38] P.F. Knowles, D. Marsh, H.W.E. Rattle, Magnetic Resonance of Biomolecules: An Introduction to the Theory and Practice of NMR and ESR in Biological Systems, Wiley-Interscience, London, 1976.
[39] P.Z. Qin, S.E. Butcher, J. Feigon, W.L. Hubbell, Quantitative analysis of the isolated GAAA tetraloop/receptor interaction in solution: a site-directed spin labeling study, Biochemistry 40 (2001) 6929–6936.
[40] A. Spaltenstein, B.H. Robinson, P.B. Hopkins, Sequence- and structure-dependent DNA base dynamics: synthesis, structure, and dynamics of site and sequence specifically spin-labeled DNA, Biochemistry 28 (1989) 9484–9495.
[41] O.K. Strobel, R.S. Keyes, A.M. Bobst, Base dynamics of local Z-DNA conformations as detected by electron paramagnetic resonance with spin-labeled deoxycytidine analogues, Biochemistry 29 (1990) 8522–8528.
[42] A.M. Portis, Electronic structure of F centers: saturation of the electron spin resonance, Phys. Rev. 91 (1953) 1071–1078.
[43] T.G. Castner Jr., Saturation of the paramagnetic resonance of a V center, Phys. Rev. 115 (1959) 1506–1515.
[44] H. Beinert, W.H. Orme-Johnson, in A. Ehrenberg, B.G. Malmström, T. Vänngård (Ed.), Magnetic resonance in biological systems; Proceedings, Symposium Publications Division, Pergamon Press, London, 1967, p.221–247.
[45] G.S. Manning, The molecular theory of polyelectrolyte solutions with applications to the electrostatic properties of polynucleotides, Q. Rev. Biophys. 11 (1978) 179–246.
[46] C. Galli, J. Innes, D. Hirsh, G. Brudvig, Effects of dipole–dipole interactions on microwave progressive power saturation of radicals in proteins, J. Magn. Reson., B 110 (1996) 284–287.
[47] M.A. O'Neill, J.K. Barton, DNA-mediated charge transport requires conformational motion of the DNA bases: elimination of charge transport in rigid glasses at 77 K, J. Am. Chem. Soc. 126 (2004) 13234–13235.
[48] C.H. Spink, J.B. Chaires, Effects of hydration, ion release, and excluded volume on the melting of triplex and duplex DNA, Biochemistry 38 (1999) 496–508.
[49] R. Bhat, S.N. Timasheff, Steric exclusion is the principal source of the preferential hydration of proteins in the presence of polyethylene glycols, Protein Sci. 1 (1992) 1133–1143.
[50] Glen Research, Amino-Modifier C2 dT, 10-1037-XX, 03/10/2007, http://www.glenres.com/.
[51] Glen Research, Carboxy-dT, 10-1035-XX, 03/10/2007, http://www.glenres.com/.
[52] C.H. Spink, N. Garbett, J.B. Chaires, Enthalpies of DNA melting in the presence of osmolytes, Biophys. Chem. 126 (2007) 176–185.
[53] O.K. Strobel, R.S. Keyes, R.R. Sinden, A.M. Bobst, Rigidity of a B-Z region incorporated into a plasmid as monitored by electron paramagnetic resonance, Arch. Biochem. Biophys. 324 (1995) 357–366.
[54] S.R. Holbrook, S.H. Kim, Local mobility of nucleic acids as determined from crystallographic data. I. RNA and B form DNA, J. Mol. Biol. 173 (1984) 361–388.
[55] H.R. Drew, S. Samson, R.E. Dickerson, Structure of a B-DNA dodecamer at 16 K, Proc. Natl. Acad. Sci. U. S. A. 79 (1982) 4040–4044.
[56] H.R. Drew, R.M. Wing, T. Takano, C. Broka, S. Tanaka, K. Itakura, R.E. Dickerson, Structure of a B-DNA dodecamer: conformation and dynamics, Proc. Natl. Acad. Sci. U. S. A. 78 (1981) 2179–2183.
[57] W. Hillen, R.D. Wells, Circular dichroism studies of the B goes to A conformational transition in seven small DNA restriction fragments containing the *Escherichia coli* lactose control region, Nucleic Acids Res. 8 (1980) 5427–5444.
[58] A.I. Poletaev, V.I. Ivanov, L.E. Minchenkova, Conformational changes within the A-family of double-stranded nucleic acids in solution, Mol. Biol. 10 (1976) 675–682.